Scaffold-Mediated Sustained, Non-viral Delivery of miR-219/miR-338 Promotes CNS Remyelination

Ulla Milbreta,[1,9] Junquan Lin,[1,9] Coline Pinese,[1,2] William Ong,[1,3] Jiah Shin Chin,[1,3] Hitomi Shirahama,[1] Ruifa Mi,[4] Anna Williams,[5] Marie E. Bechler,[5] Jun Wang,[6,7] Charles ffrench-Constant,[5] Ahmet Hoke,[4] and Sing Yian Chew[1,8]

[1]School of Chemical and Biomedical Engineering, Nanyang Technological University, Singapore 637459, Singapore; [2]Artificial Biopolymers Department, Max Mousseron Institute of Biomolecules (IBMM), UMR CNRS 5247, University of Montpellier, Faculty of Pharmacy, Montpellier 34093, France; [3]NTU Institute for Health Technologies (Health Tech NTU), Interdisciplinary Graduate School, Nanyang Technological University, Singapore 637533, Singapore; [4]Department of Neurology, Johns Hopkins University School of Medicine, Baltimore, MD 21205, USA; [5]MRC-Centre for Regenerative Medicine, University of Edinburgh, 5 Little France Drive, Edinburgh EH164UU, Edinburgh, UK; [6]China School of Biomedical Science and Engineering, South China University of Technology, Guangzhou International Campus, Guangzhou 510006, P. R. China; [7]National Engineering Research Center for Tissue Restoration and Reconstruction, South China University of Technology, Guangzhou 510006, P. R. China; [8]Lee Kong Chian School of Medicine, Nanyang Technological University, Singapore 308232, Singapore

The loss of oligodendrocytes (OLs) and subsequently myelin sheaths following injuries or pathologies in the CNS leads to debilitating functional deficits. Unfortunately, effective methods of remyelination remain limited. Here, we present a scaffolding system that enables sustained non-viral delivery of microRNAs (miRs) to direct OL differentiation, maturation, and myelination. We show that miR-219/miR-338 promoted primary rat OL differentiation and myelination in vitro. Using spinal cord injury as a proof-of-concept, we further demonstrate that miR-219/miR-338 could also be delivered non-virally in vivo using an aligned fiber-hydrogel scaffold to enhance remyelination after a hemi-incision injury at C5 level of Sprague-Dawley rats. Specifically, miR-219/miR-338 mimics were incorporated as complexes with the carrier, TransIT-TKO (TKO), together with neurotrophin-3 (NT-3) within hybrid scaffolds that comprised poly(caprolactone-co-ethyl ethylene phosphate) (PCLEEP)-aligned fibers and collagen hydrogel. After 1, 2, and 4 weeks post-treatment, animals that received NT-3 and miR-219/miR-338 treatment preserved a higher number of Olig2$^+$ oligodendroglial lineage cells as compared with those treated with NT-3 and negative scrambled miRs (Neg miRs; p < 0.001). Additionally, miR-219/miR-338 increased the rate and extent of differentiation of OLs. At the host-implant interface, more compact myelin sheaths were observed when animals received miR-219/miR-338. Similarly within the scaffolds, miR-219/miR-338 samples contained significantly more myelin basic protein (MBP) signals (p < 0.01) and higher myelination index (p < 0.05) than Neg miR samples. These findings highlight the potential of this platform to promote remyelination within the CNS.

INTRODUCTION

Oligodendrocytes (OLs), glial cells that form the myelin sheaths within the CNS,[1] are essential for facilitating saltatory signal conduction in axons, as well as providing metabolic support for neuronal survival.[2,3] Without myelin ensheathment, energy-efficient conduction in axons cannot occur, which in turn results in perturbed axonal transport, degeneration, and ultimately functional impairment.[4] The importance of this structure was further displayed in patients with non-penetrating traumatic nerve injuries in the CNS, where even though a portion of axons was spared post-injury, functional recovery was still not observed due to demyelination.[5] This suggests that although regeneration of axons is an end goal, they have to be myelinated in order to allow proper conduction of nerve impulses.

Within the spinal cord, OL progenitor cells (OPCs) exist endogenously, and they continue to proliferate and differentiate into myelinating OLs in the adult CNS after injury. Much evidence suggests that OPCs residing in the white matter of the spinal cord represent the largest potential source of remyelinating OLs.[6] However, although the proliferation rate of OPCs increases significantly post-spinal cord injury (SCI), spontaneous remyelination remains limited, particularly in humans.[7] Because pre-existing damaged OLs do not contribute to remyelination,[8,9] current strategies to encourage myelin regeneration include either transplantation of exogenous cells into the injury site[10] or activation of the endogenous pool of OPCs. Although both approaches are feasible and have been demonstrated, the former method may present more issues because the availability of autologous OPCs is limited, and heterologous transplantation requires long-term immunosuppression that may cause serious side effects.[10]

As such, we focus on the latter. Early in vitro culture experiments involving primary OPCs from post-natal CNS indicated that in the absence of signals to maintain the cells as OPCs, they would rapidly differentiate into OLs.[11] This suggests that much of the regulation

in CNS myelination might be at the level of inhibiting this otherwise default pathway of differentiation, and the relief of inhibition might lead to OL differentiation and myelination.[11] Hence strategies that aim to silence some of these inhibitory pathways may promote re-myelination in the CNS.

MicroRNAs (miRs) are small non-coding RNAs (21–23 bp) that are involved in gene expression regulation via RNAi.[12] They are intricately involved in directing the fate of OPCs and OLs. Specifically, microRNA-219 (miR-219) and microRNA-338 (miR-338) are effective in promoting OPC differentiation *in vitro* and *in vivo* by suppressing the expression of gene targets that promote OPC proliferation.[13–16] Furthermore, in a recent study, Wang et al.[17] demonstrated that these miRs have a synergistic role in enhancing myelin repair in an experimental demyelinating model induced by lysolecithin (LPC). Building on their well-substantiated findings, we sought to improve the delivery method of these miRs for long-term therapeutic purposes, using SCI as a proof-of-concept and an extended application. Importantly, although both of these models can induce demyelination, SCI presents a higher level of difficulty because of the plethora of factors that impede myelin formation around the injured region.[18]

Therefore, in this study, we fashioned a fiber-hydrogel scaffold for non-viral sustained delivery of both miR-219 and miR-338 (miR-219/miR-338) *in vivo*. Specifically, this hybrid scaffold consisted of a core bundle of aligned poly(caprolactone-co-ethyl ethylene phosphate) (PCLEEP) fibers, which were structurally stabilized in a three-dimensional (3D) configuration by collagen hydrogel embedment. Within the collagen hydrogel, miRs and drugs can be loaded and delivered through diffusion to the microenvironment. Having established its efficacy in concurrently delivering miRs and neurotrophins,[19] as well as providing topographical cues to enhance axonal regeneration,[19,20] we proceeded to assess the effects of this scaffold on OPC differentiation and myelin regeneration *in vivo* using a spinal cord C5 hemi-incision rodent model. Here, we show that rats implanted with miR-219/miR-338-loaded scaffolds retained a higher population of oligodendroglial lineage cells around the lesion site. These cells also displayed enhanced differentiation capabilities and myelinated more axons. Altogether, the results highlight the potential of these miR-incorporated fiber-hydrogel scaffolds in enhancing the survival of OPCs and promoting myelination within the injured CNS.

RESULTS

Fiber-Mediated Non-viral Delivery of miR-219/miR-338 Enhanced OPC Differentiation and Myelination *In Vitro*

The efficacy of using a fiber platform to transfect primary rat OPCs non-virally with miR-219/miR-338 and the corresponding enhanced cellular differentiation and maturation were demonstrated *in vitro* previously.[14] However, the functionality of an OL is determined by its ability to wrap and myelinate. Hence, extending from our recent work, where initial OL myelin ensheathment was evaluated at day 7,[21] we assessed the myelination outcomes at an extended culture period of 14 days in this work. As shown in Figures 1A–1C, miR-219/miR-338 treatment significantly enhanced OPC differentiation

and maturation when cells were cultured in myelin medium, resulting in larger numbers of myelin basic protein-positive (MBP$^+$) mature OLs per Olig2$^+$ oligodendroglial lineage cells as compared with negative scrambled miR (Neg miR) transfection (85.1% ± 5.1% versus 59.1% ± 9.4%; p < 0.01). This reinforced the efficacy of miR-219/miR-338 in enhancing OPC differentiation and maturation under both proliferative[14] and pro-myelinogenic conditions. Besides that, miR-219/miR-338 also markedly increased the myelin sheath length on the fibers as compared with the Neg miR control (Figures 1A and 1D). Further quantification of myelin sheath formation revealed that miR-219/miR-338 led to more complete-looking myelin structures per OL (on average, 2.4 ± 1.5 numbers of sheaths per cell; Figure 1E) as opposed to Neg miR treatment, which resulted in only 0.5 ± 0.9 number of sheaths per cell. Additionally, 88.6% of MBP$^+$ cells in the miR-219/miR-338 group had complete myelin sheath formation, whereas only 34.3% of MBP$^+$ cells in the scrambled Neg miR group produced complete sheaths. Because we did not detect the formation of complete sheaths from either sample at earlier time points (day 7),[21] it is likely that the sheaths in the Neg miR group failed to form properly instead of breaking down during the course of the experiment.

Sustained Release of NT-3 and miRs from Fiber-Hydrogel Scaffolds

A sustained availability of drugs may be desirable because OPCs require at least 14 days to differentiate, ensheathe, and form compact myelin.[22] Hence a scaffold was designed to deliver drugs in a sustained and localized fashion. In particular, neurotrophin-3 (NT-3), a neurotrophic factor that is commonly used for enhancing neuronal survival,[23] was delivered together with miR-219 and miR-338.[19] In addition, the scaffold was designed to provide topographical guidance to regenerating axons through the means of aligned fibers, as shown in Figures 2A and 2B. Using characterization methods described previously,[14,19] we observed that both NT-3 (loading efficiency of 6.23%) and miR-loaded (loading efficiency of 28.91%) scaffolds displayed burst release profiles within the first 1 hr, where ∼10% of the actual experimental amounts were released (Figure 2C). For the next 20 days, 70% of NT-3 and 65% of miRs that were successfully loaded were released. Thereafter, the release of NT-3 and miRs started to plateau at day ∼60 (Figure 2C; Figure S1). Scaffold degradation study revealed a steady mass loss of the entire scaffold over time, up to approximately 60% in 30 days (Figure 2D).

Scaffold-Mediated Delivery of miR-219/miR-338 Preserved the Number of Oligodendroglial Lineage Cells around Injury Site after SCI

Having established that scaffold-mediated non-viral delivery of miR-219/miR-338 could enhance OL differentiation and myelination *in vitro*, we next assessed the *in vivo* therapeutic efficacy of this approach using a hemi-incision SCI model as a proof-of-concept. In our opinion, this C5 hemi-incision model was most suitable because it is well established and surgically reproducible. We first evaluated whether scaffold-mediated delivery of miR-219/miR-338 would elicit effects on the total cell numbers around the lesion site
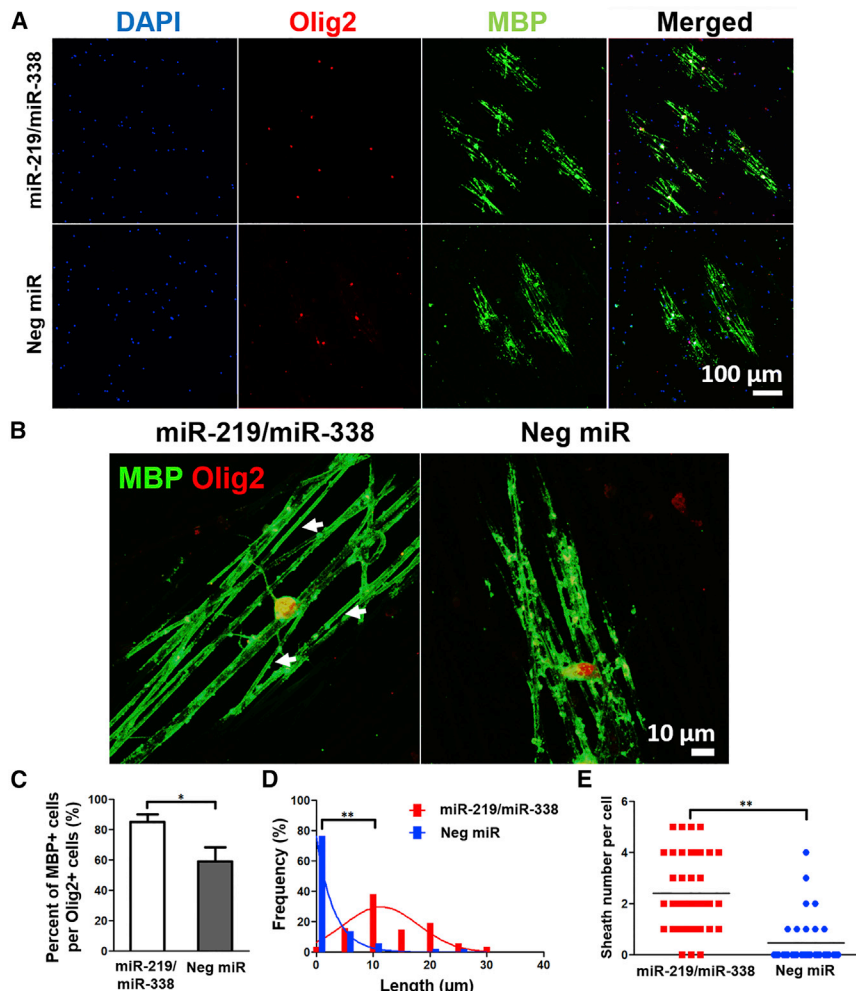
Figure 1. Scaffold-Mediated Delivery of miR-219/miR-338 Promoted OPC Differentiation and Myelination *In Vitro*

(A) Representative confocal images show that cocktail of miRs promoted differentiation of OPCs into MBP+ OL after 2 weeks. Scale bar represents 100 μm. (B) Representative confocal images show that cocktail of miRs increased the length and number of complete myelin sheath per OL after 2 weeks. Scale bar represents 10 μm. (C) Quantitative data show miR-219 and miR-338 treatment resulted in more MBP+ cells per Olig2+ cells. ANOVA with Tukey's *post hoc* test; at least 100 cells were quantified per sample group in each experiment repeat (n = 3 independent experiments). *p < 0.01. (D) Quantitative data show miR-219 and miR-338 treatment resulted in significant differences between the average sheath length. (E) Quantitative data show miR-219/miR-338 treatment resulted in higher average number of compact myelin sheath per OL. Each dot represents one cell. **p < 0.001, two-tailed t test; 40 cells in the miR-219/miR-338 group and 35 cells in the NEG miR group, from three independent experiments.

Scaffold-Mediated Delivery of miR-219/miR-338 Promoted OPC Differentiation after SCI

We next examined the maturity of the Olig2+ cell population around the lesion site because miR-219/miR-338 overexpression has been reported to enhance OPC differentiation *in vitro*[13,14] and *in vivo*, albeit in a development model.[15,16] The expression of platelet-derived growth factor receptor alpha (PDGFRα), a cell-surface marker that is expressed by OPCs, but not mature OLs,[2] was assessed at weeks 1, 2, and 4 post-implantation to track the number of OPCs over time. Quantification results showed significant reduction in PDGFRα+ cell density from week 1 to 4 for both treatment groups (440 to 180 cells/mm² for the miR-219/miR-338 group and 410 to 200 cells/mm² for the Neg miR group; p < 0.001) (Figures 4A and 4B). When comparing miR-219/miR-338 and Neg miR-treated animals within a specific time point, no significant difference was observed (Figure 4B).

In order to validate these findings, we next evaluated the expression of CC-1, a protein marker that is predominantly found in mature OLs but absent in OPCs.[25] Complementary to the trend that was observed in PDGFRα expression, CC-1+ cell density around the injury area increased from week 1 to 4 for both treatment groups (1,050–1,770 cells/mm² in the miR-219/miR-338 group and 1,050–1,380 cells/mm² in the Neg miR group) (Figures 4C and 4D). However, the degree of OL differentiation appeared more extensive in the presence of miR-219/miR-338. In particular, significantly more CC-1+ mature OLs were observed when animals received miR-219/miR-338 after 2 and 4 weeks of treatment (p < 0.05 and p < 0.01,

(Figure 3A). Specifically, we quantified the number of DAPI+ cells and found that there was no significant difference in the total cell number between the two treatment groups at all time points (Figures 3B and 3C). Next, we asked whether miR-219/miR-338 would affect the number of oligodendroglial lineage cells, which would include OPCs and OLs, around the lesion site through the analysis of Olig2 expression.[24] We found that miR-219/miR-338 treatment maintained a consistent number of Olig2+ cells at weeks 1, 2, and 4 post-implantation. On the contrary, significant changes were observed in animals that received non-functional, Neg miR treatment. Specifically, at week 1 post-implantation, the densities of Olig2+ cells around the peri-lesion site were similar between both groups (2,410 cells/mm² in the miR-219/miR-338 group and 2,520 cells/mm² in the Neg miR group) (Figures 3B and 3D). However, by week 2 post-implantation, the number of Olig2+ cells decreased significantly in the Neg miR group, and this number remained consistently low after 4 weeks of recovery. For both of these time points, we observed significantly higher Olig2+ cell densities in the miR-219/miR-338 group as compared with the Neg miR group (p < 0.001) (Figures 3B and 3D).
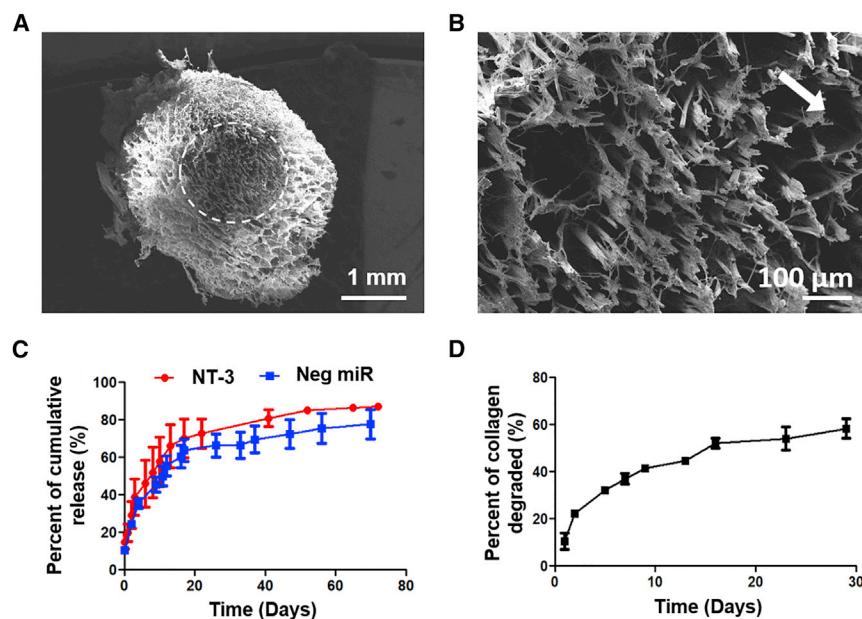
Figure 2. Fiber-Hydrogel Scaffold for Sustained Non-viral Drug and/or Gene Delivery

(A) Scanning electron microscopy images of cross-section of scaffold showing aligned electrospun fibers and collagen matrix. Scale bar represents 1 mm. (B) Magnified image of aligned electrospun fibers (white arrow indicates the direction of fiber alignment, which points out of the page at ~45°). Scale bar represents 100 μm. (C) Cumulative release of miR and NT-3 over time. (D) Mass loss of scaffold over time. Data are represented as mean ± SD.

along with 2′,3′-cyclic nucleuotide-3′-phospho-diesterase (CNPase), for validation at 4 weeks post-implantation. Under the fluorescence microscope, MBP and CNPase signals were identifiable in the tissues and within the implants as shown in Figure 5A. By quantifying the percentage of area of the scaffold that possessed MBP+ signals, we found that MBP expression was more extensive in scaffolds that incorporated miR-219/miR-338 (MBP+ area = 45.73% ± 4.74%) as compared with Neg miR samples (MBP+ area = 20.92% ± 2.77%) (Figure 5B).
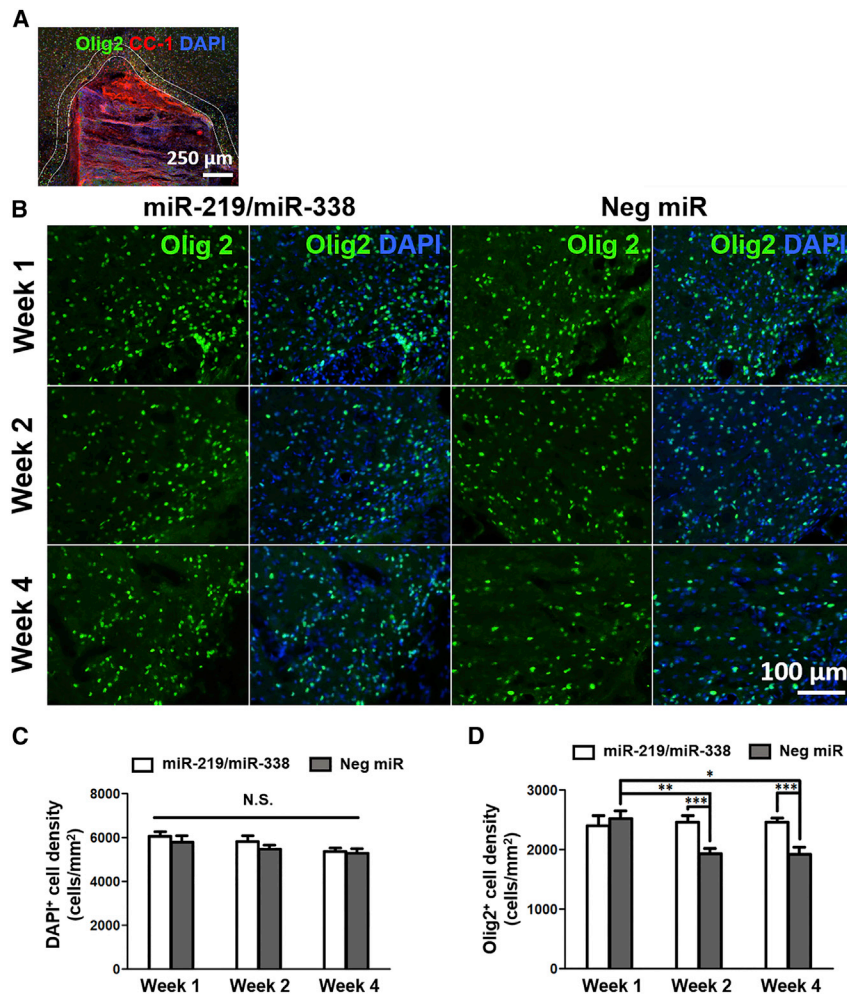
We next proceeded to evaluate the extent of myelination within the scaffolds by quantifying the myelination index (defined as the percentage of colocalization of MBP with axonal NF200). In particular, we found that miR-219/miR-338-treated animals (60.51% ± 4.99%) displayed significantly higher myelination index than Neg miR-treated animals (32.06% ± 7.54%; p < 0.05) (Figures 5C and 5D). Because OLs were also able to myelinate electrospun fibers *in vitro*, we wanted to know whether the fibers within the scaffold were myelinated in an *in vivo* setting. Surprisingly, from the transmission electron microscopy (TEM) images, we were unable to identify any compact myelin structures around the electrospun fibers in both of the treatment groups (Figure S3).

Additionally, we also analyzed the host-implant interface for potential signs of myelination. At week 4 post-implantation, we observed MBP+ tubular structures that surrounded NF+ axons at the host-implant interface for both miR-219/miR-338 and Neg miR-treated animals (Figure 6A). We then quantified the myelination index and found a trend that suggested better myelination outcomes in the presence of miR-219/miR-338 (13.65% ± 1.77% versus 9.49% ± 2.99% for Neg miR treatment; Figure 6B). Finally, further analyses using TEM showed that compact myelin formation (Figure 6C) could be detected in animals that received miR-219/miR-338. In contrast, these structures were absent in animals that received Neg miR treatment (Figure 6D).

respectively, versus Neg miR; Figure 4D). Besides enhancing the extent of OL differentiation, miR-219/miR-338 treatment also appeared to increase the rate of OL differentiation. Specifically, significantly larger numbers of mature CC-1+ OLs were detected starting 2 weeks post-implantation of miR-219/miR-338 scaffolds. This number of mature OLs continued to increase after 4 weeks of recovery. In contrast, animals that received Neg miR treatment showed significant increase in the number of mature CC-1+ OLs only after 4 weeks post-implantation. Taken together, the results suggest that PDGFRα+ cells lost their viability over time following SCI. However, as indicated by the CC-1+ cell numbers, those cells that survived could be aided by the miR treatment, hence resulting in enhanced OL differentiation and maturation.

Previously, NT-3 was demonstrated to stimulate OPC proliferation[26–28] and maturation.[28] Because all of our scaffolds contained NT-3 along with miRs, to confirm that the results obtained were indeed due to the effects of miR-219/miR-338, we included another treatment group that received only NT-3, without the addition of miRs, for comparison at week 2 post-implantation. The results showed that NT-3 did not lead to any significant changes in both Olig2+ and CC-1+ cell populations as compared with Neg miR treatment (Figure S2). Instead, for both of these cell populations, significant differences were detected only between miR-219/miR-338 and NT-3 groups, as well as between miR-219/miR-338 and Neg miR groups.

Scaffold-Mediated Delivery of miR-219/miR-338 Enhanced Myelin Formation after SCI

The microenvironment of the injured area within the spinal cord is very inhibitive for myelin formation.[29] To determine the extent of myelin regeneration after injury, we stained the samples with MBP,

Scaffold-Mediated Delivery of miR-219/miR-338 Did Not Affect Neurite Outgrowth or Exacerbate Glial Scarring after SCI

Although the fiber-hydrogel scaffold provided localized drug delivery,[19] the transfection of miRs was still non-specific at the implant

Figure 3. Scaffold-Mediated Non-viral Delivery of miR-219/miR-338 Preserved Oligodendroglial Lineage Cell Numbers after SCI

(A) Representative image of scaffold implanted in injury site. Double white lines around the scaffold delineate the perilesion region where quantifications were conducted. Scale bar represents 250 µm. (B) Olig2$^+$ cells (green) in the miR-219/miR-338 treatment group (left) and Neg miR group (right). Scale bar represents 100 µm. (C) DAPI$^+$ cell density remained consistent at perilesion area after SCI regardless of scaffold treatment. (D) Olig2$^+$ cell density remained consistent at perilesion area in the presence of miR-219/miR-338 but decreased significantly under treatment with Neg miR. ***$p < 0.001$; **$p < 0.01$; *$p < 0.05$; N.S., not significant (ANOVA). Data are represented as mean ± SEM.

DISCUSSION

Axon demyelination within the CNS, regardless through mechanical injuries or pathological consequences, usually results in functional impairments that can severely affect a patient's quality of life. Yet, effective remyelination strategies remain limited. Besides being a keystone cell type for restoring energy-efficient signal conduction in axons, OLs are also crucial in providing metabolic support for axonal survival. Unfortunately, the injured CNS is often not permissive for myelin regeneration due to the plethora of inhibitory factors that are present.[18,29] Despite that, it may be possible to bypass this restriction if a potent method to drive robust myelin regeneration exists. Correspondingly, this study highlights the use of scaffold-mediated non-viral delivery of miR-219/miR-338 to promote *in vivo* CNS remyelination, using SCI as a proof-of-concept.

and/or injury site. Hence we proceeded to investigate the effects of the scaffolds on neurite outgrowth and glial scarring.

We observed that regardless of miR treatment, no significant difference was detected in NF200 signals at the host-implant interface (Figures S4A and S4B), as well as within the scaffolds (Figures S4A and S4C). These observations were consistent with our *in vitro* results where the well-established and robust DRG neuronal culture was used. Specifically, *in vitro* transfection of DRG neurons showed that the non-viral transfection of miR-219/miR-338 had no significant impact on the extents of neurite outgrowth as compared with untreated cells, cells treated with Neg miR, or the transfection reagent, TransiT-TKO (TKO), alone (Figure S5).

In the case of glial scarring, when the intensity of glial fibrillary acidic protein (GFAP; a positive indicator of glial scar formation by activated astrocytes[30]) was analyzed at the perilesion region, no significant difference was detected between miR-219/miR-338 and Neg miR-treated groups at all time points (Figure S6).

Previous works by several groups have identified miR-219 and miR-338 to be responsible for regulating the maturation and myelination of cells from the oligodendroglial lineage.[15,16,31] Moreover, a recent work by Wang et al.[17] showed that miR-219 and miR-338 have additive effects on OPC differentiation and are required for the full extent of myelination. Mechanistically, these two miRs exert their effects by inhibiting a set of OPC differentiation-inhibiting genes such as PDGFRα, SRY-box containing gene (Sox6), forkhead box J3 (FoxJ3), zinc-finger protein 238 (ZFP238), and Hes5.[15–17] Hes5, in particular, is a critical downstream effector within the Notch signaling pathway and has also been shown to be related to the expression of myelin markers.[32,33] From developmental studies, it was observed that Hes5 levels were elevated in naive OPCs and progressively decreased as they differentiated and started to express myelin genes.[32,33] The rest of the inhibitory genes mentioned were demonstrated to be similarly regulated in our past studies, which investigated
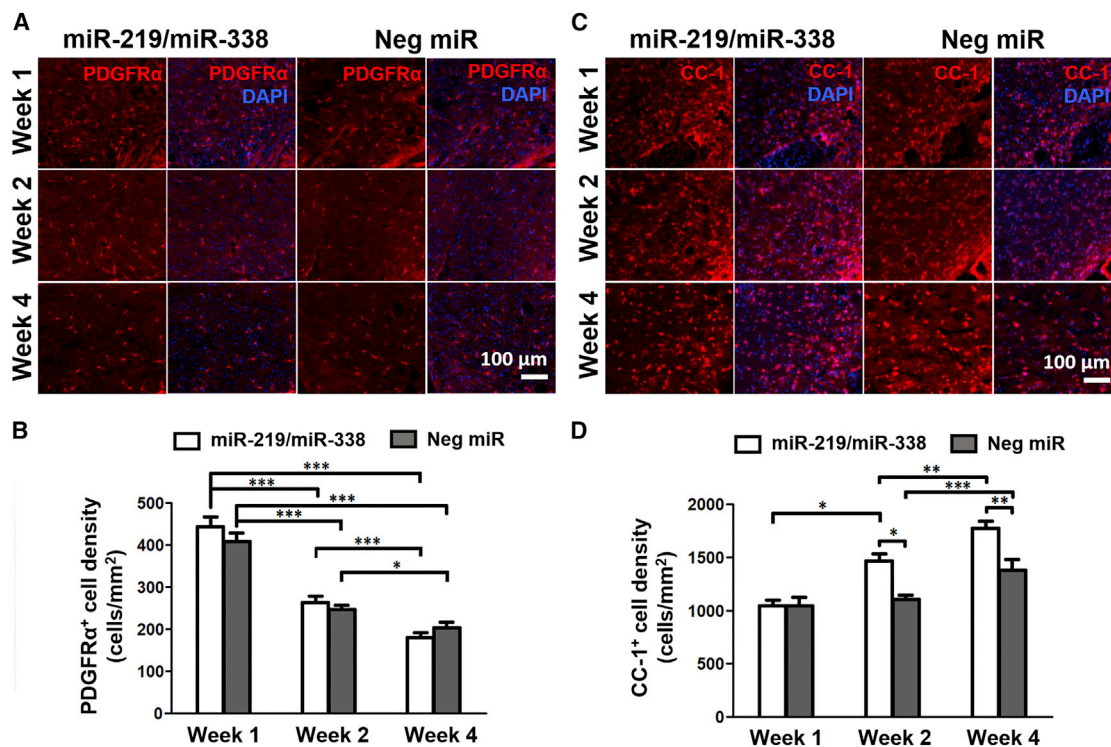
Figure 4. Scaffold-Mediated Non-viral Delivery of miR-219/miR-338 Promoted Greater Extent and Rate of OPC Differentiation

(A) PDGFRα+ cells (red) in the miR-219/miR-338 treatment group (left) and Neg miR group (right). Scale bar represents 100 μm. (B) Density of PDGFRα+ cells per perilesion area. (C) CC-1+ mature OLs (red) in the miR-219/miR-338 treatment group (left) and Neg miR group (right). Scale bar represents 100 μm. (D) Density of CC-1+ cells per perilesion area. ***p < 0.001; **p < 0.01; *p < 0.05 (Kruskal-Wallis, Mann-Whitney U test). Data are represented as mean ± SEM.

the effects of sustained fiber-mediated delivery of miR-219 and miR-338 on OPC differentiation.[13,14]

Here, we hypothesized that a combination of scaffold topography and RNAi would prime the endogenous population of OPCs to engage in myelination after injuries within the CNS. We first explored the effects of miR-219/miR-338 cocktail on OPC differentiation and myelination *in vitro* using electrospun PCL fibers. These fibers were fabricated to be suspended,[21] unlike those used in our previous work,[14] which were condensed to form a fibrous mat. However, because the miR loading strategy was similar, we would also anticipate a burst release within the first week and subsequent sustained release for another week.[14] Consistent with previous *in vitro* findings, OPCs matured faster when transfected with miR-219/miR-338 as indicated by the increased percentage of cells expressing MBP at week 2. The effect of these miRs' gene silencing, using this platform, has also been confirmed in those studies.[13,14] Besides that, we also demonstrated that this miR cocktail could greatly enhance the ensheathment length and number of sheaths that were formed by MBP+ OLs after 2 weeks of differentiation. The quantification method for counting the number of sheaths per cell in this paper was adopted from a previous study by Bechler et al.[22] Compared with their measurements, the number of complete sheaths we obtained were 2- to 3-fold less.

This observation may be because of the process of miR transfection, which may be more cytotoxic to sensitive cells like OPCs and OLs.

The scaffold utilized in this *in vivo* study contained two important features, aligned electrospun fibers and collagen hydrogel. This design was adopted from our previous study where aligned electrospun fibers were employed to provide topographical guidance for axon ingrowth.[19,20] These fibers were also arranged in a 3D conformation so as to imitate the architecture of the natural extracellular matrix and allow infiltrating cells to maintain their viability.[34] To keep these fibers intact during and after implantation, we added collagen hydrogel for physical support. Importantly, another role played by collagen hydrogel was the non-viral and localized sustained delivery of drugs, which has been shown in our previous works[19,20] and in this study (Figure 2C). However, unlike previous work,[19] we decreased the concentration of the collagen hydrogel and also varied the transfection reagent for miR delivery in this study. Of note, we found that oligonucleotides were taken up by cells in the surrounding tissues, up to a distance of 300 μm.[19] Hence we chose a distance of 100 μm away from the borders of our scaffold for analysis of cellular response as we would expect an increase of myelin under the influence of the miRs. This analysis of cellular response at the perilesion region is also consistent with the literature.[35]
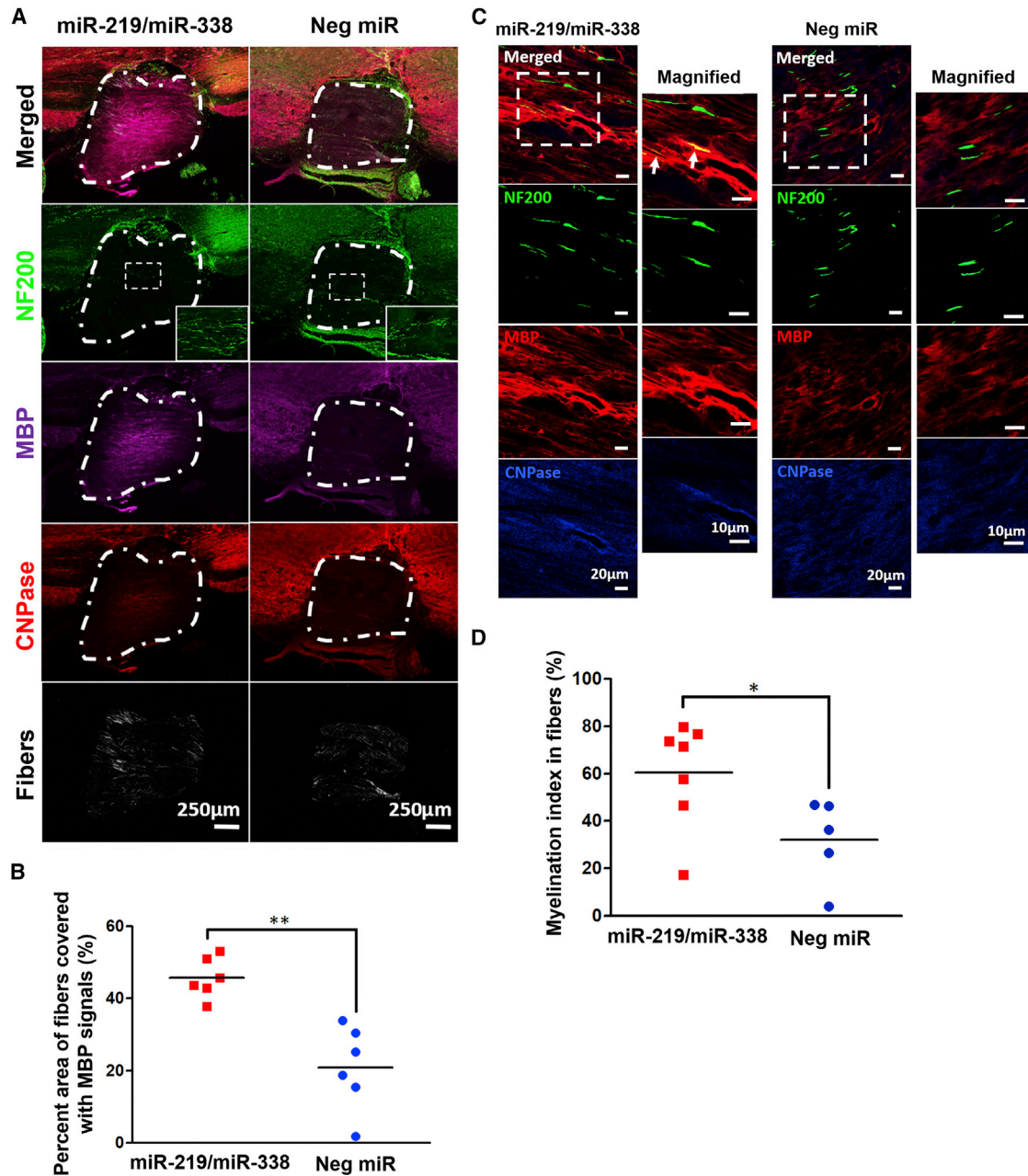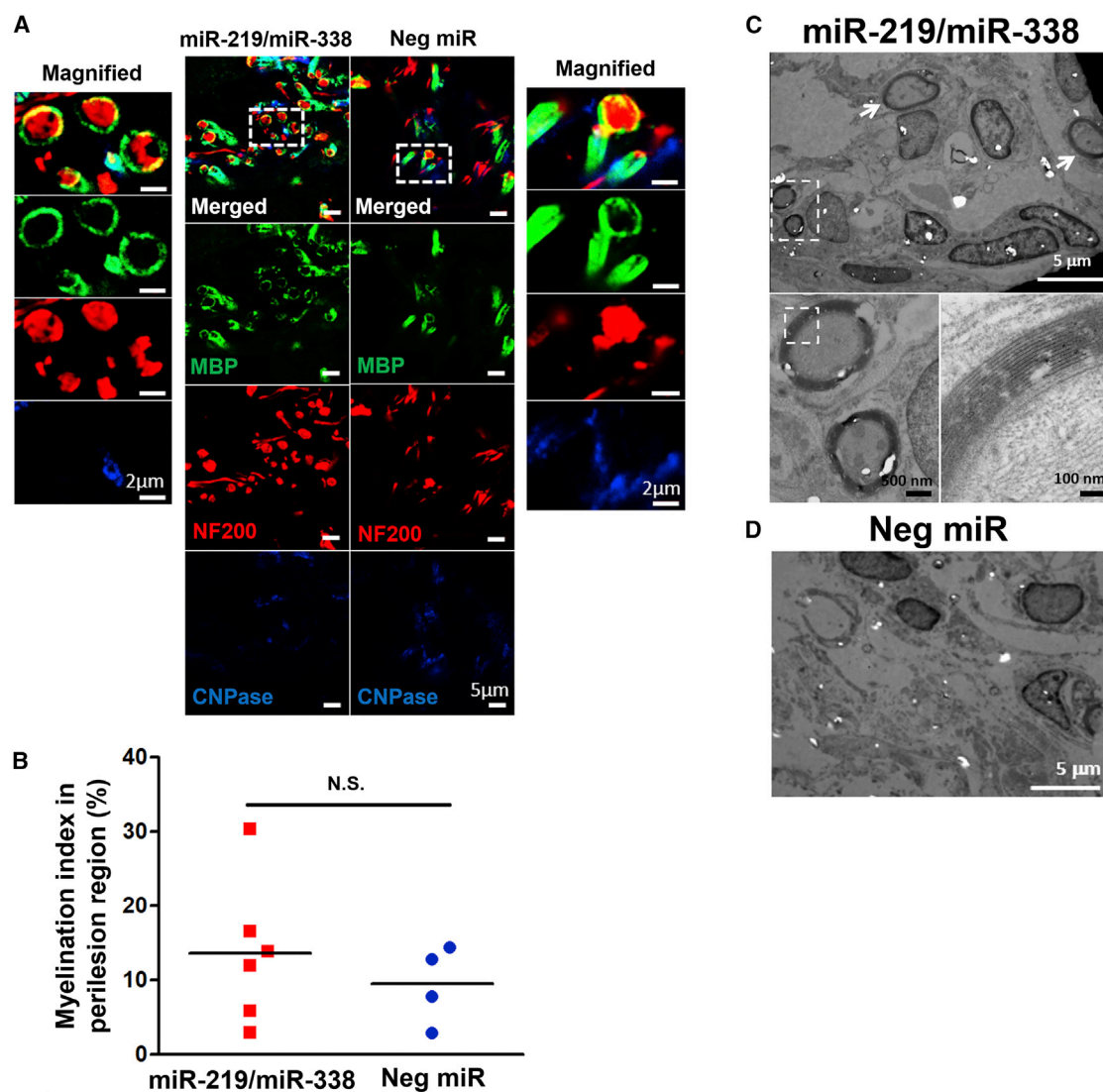
Figure 5. Scaffold-Mediated Non-viral Delivery of miR-219/miR-338 Supported Myelin Regeneration and Axon Ensheathment within Scaffold

(A) Representative images comparing different miR-219/miR-338- and Neg miR-loaded scaffolds. Relatively prominent MBP and CNPase signals were observed within scaffolds with miR-219/miR-338 at week 4. White dotted lines demarcate the region occupied by the scaffold. Scale bar represents 250 μm. (B) Percent of fiber-scaffold area that is MBP+. (C) Representative images from week 4 samples showing MBP+ signals in scaffold. White arrows indicate axons that appeared to be partially ensheathed. Scale bar represents 20 μm in the normal images and 10 μm in the magnified images. (D) Myelination index obtained within the scaffolds. **p < 0.01, *p < 0.05 (Student's t test).

In our attempt to characterize the density of oligodendroglial lineage cells around the perilesion site, we observed notable differences in the number of Olig2+ cells between miR-219/miR-338 and Neg miR treatment groups from 2 weeks post-implantation onward. When comparing the perilesional density of Olig2+ cells between miR-219/miR-338 and Neg-miR treatment groups, some differences were observed during weeks 2 and 4 post-injury. Based on the consistent density of DAPI+ cells during the entire duration of the experiment, these results indicated that miR-219/miR-338 might be able to preserve the viability of oligodendroglial lineage cells. Due

Figure 6. Scaffold-Mediated Non-viral Delivery of miR-219/miR-338 Showed a Trend of Enhanced Myelination at Host-Implant Interface

(A) Representative images obtained at week 4 depicting MBP$^+$ tubular structures surrounding NF$^+$ axons. Scale bar represents 5 μm in the normal images and 2 μm in the magnified images. (B) Myelination index obtained at host-implant interface. (C and D) Representative transmission electron microscopy images showing the (C) presence and (D) lack of myelinated axon formation in (C) miR-219/miR-338 and (D) Neg miR groups, respectively. Scale bars for the TEM images are labeled with their respective scale bar size. N.S., not significant (Student's t test).

to limited literature investigating the effects of miR-219/miR-338 on OPC cell survival, further confirmation of this observation would require lineage tracing of OPCs.[36]

Axon myelination within the injured CNS is an important element of regeneration.[36] Consistent with a recent study by Wang et al.,[17] albeit in a non-SCI model, we observed similar trends where miR-219/miR-338 treatment led to a higher number of axons being myelinated as compared with Neg miR treatment (Figure 6). Besides examining OPCs/OLs, we also assessed the effects of miR-219/miR-338 on neurons and astrocytes. Previously, we showed that this scaffold platform

could deliver other miRs, such as miR-222, to enhance axonal regeneration *in vivo*.[19] Therefore, the lack of significant differences in neurite length between miR-219/miR-338 and Neg miR groups *in vivo* (Figure S4) and *in vitro* (Figure S5) indicated that it was most likely due to the insensitivity of neurons and/or axons toward miR-219/miR-338 and not due to the failure of miR uptake and/or delivery. The same conclusion can be drawn for results observed in astrocytes where glial scarring was not significantly induced in both miR-219/miR-338 and Neg miR-treated groups. However, because GFAP is indicative of only astrocyte activation,[30] there might be other secretory factors that led to a more permissive environment for myelin

regeneration. Future studies could be conducted to investigate this hypothesis.

OLs were shown to be able to myelinate electrospun fibers *in vitro*.[22,37] However, when we sectioned the scaffolds and examined them under the TEM, we did not observe any fiber ensheathment *in vivo* (Figure S3). Based on a recent study by Assinck et al.,[36] we speculate that one possible reason could be that the OPCs within the scaffolds were differentiating into Schwann cells instead of OLs. Contrary to OLs, there are not many studies demonstrating the potential of Schwann cells in ensheathing electrospun fibers *in vitro* and *in vivo*. Moreover, it has been shown previously that Schwann cell myelination is regulated by signaling molecules, such as Neuregulin 1 type III.[38,39] Because our fibers were not coated with myelination cues, they were unlikely to be myelinated. Hence future works could explore the effects of miR-219/miR-338 on OPC differentiation into Schwann cells versus OLs. Importantly, we would also seek to elucidate the relative potential of OLs and Schwann cells in inducing myelin regeneration and subsequent functional recovery after SCI.

RNAi is widely adopted in treatments related to cancer therapy and genetic diseases. However, it presents much wider implications and is potentially useful in regenerative medicine. Unfortunately, one of the major stumbling blocks to the translational use of RNAi is the development of proper delivery systems for effective and efficient *in vivo* delivery of these molecules with minimal off-target effects. Traditional approaches of systemic delivery for cancer and genetic disease therapy may not be directly beneficial to traumatic tissue injuries because the latter often involves confined injuries that also require the reestablishment of *in vivo* tissue structures. Scaffold-mediated delivery, as highlighted here, represents a potential approach because scaffolds can provide the necessary structural support and directional cues for tissue regrowth and restructuring. Furthermore, scaffold-mediated delivery of drugs provides localized delivery to the site of injury,[19] hence minimizing off-target systemic effects. Therefore, results from this work will highlight the importance of RNAi and scaffold-mediated gene silencing to regenerative medicine. This study further enforces the potential of RNAi in directing the differentiation of endogenously recruited progenitor cells. Such aspects have not been demonstrated to date.

Clinically, the implantation of similar biocompatible scaffolds for SCI treatment has already gained momentum,[40,41] and results have, thus far, shown great promise. We believe that in due time as the regulatory bodies are convinced of scaffold implantation as a treatment option for SCI or even demyelinating diseases, this work can be the next step forward to attain a higher resolution therapeutic avenue.

Conclusions

Our current study reflects the potency of scaffold-mediated delivery of miR-219/miR-338 in affecting the fate of oligodendroglial lineage cells to differentiate from OPCs to matured OLs. Furthermore, we also demonstrated that such non-viral, localized, and sustained delivery of miR-219/miR-338 could promote myelination within the injured CNS.

MATERIALS AND METHODS

2,2,2-Trifluoroethanol (TFE), heparin, BSA, horse serum, poly-D-lysine, cytosine arabinoside, 5-fluoro-2′-deoxyuridine, DNase, progesterone, putrescine, and ITS liquid media supplement (ITS) were obtained from Sigma, USA. Rat tail collagen type 1 was purchased from Corning, USA. NT-3 and nerve growth factor (NGF) were procured from PeproTech, USA. Negative scrambled microRNA (Neg miR), miR-219, miR-338-3p, miR-338-5p, Quant-iT RiboGreen, collagenase type 1, goat anti-mouse Alexa Fluor 555, goat anti-rat Alexa Fluor 555, goat anti-rat Alexa Fluor 633, goat anti-rabbit Alexa Fluor 488, goat anti-chicken Alexa Fluor 488, DAPI, N-2 supplement, laminin mouse protein (laminin), goat serum, Neurobasal medium, DMEM (high glucose, L-glutamine, pyruvate), GlutaMAX supplement, and penicillin-streptomycin (Pen/Strep) were acquired from Life Technologies, USA. TKO was obtained from Mirus Bio, USA. Tris-EDTA (TE) buffer (pH 8.0) and PBS (pH 7.4) were purchased from 1st Base, Singapore. NT-3 ELISA kit was bought from R&D Systems, USA. Mouse anti-CC-1 (ab16794) was obtained from Abcam, UK. Rabbit anti-Olig2 (AB9610) was acquired from Merck, USA. Rat anti-MBP (MCA409S) was purchased from Bio-Rad, USA. Chicken anti-NF200 (822601) and mouse anti-βIII-tubulin (801202) were procured from BioLegend, USA. Mouse anti-CNPase (AMAb91072) was bought from Atlas Antibodies, Sweden. Rabbit anti-GFAP (Z033401) was obtained from DAKO, Denmark. DMEM/F12 medium was purchased from Lonza, Switzerland. Papain (LS003126) was bought from Worthington Biochemical Corporation, USA.

Cell Culture

Postnatal day 0 (P0) to P2 neonatal rat cortices, along with their meninges, were removed and enzymatically digested with 1.2 U papain and 40 μg/mL DNase at 37°C for 1 hr. Thereafter, 8 mL of DMEM containing 10% fetal bovine serum (FBS) was added, and the dissociated tissues were triturated with 21G needle and syringe. Tissues from six digested cortices were seeded onto four poly-D-lysine (PDL)-coated T75 flasks and cultured in DMEM with 10% FBS and 1% Pen/Strep. After 9–11 days, the mixed glia culture was placed on an orbital shaker at 200 rpm for 1 hr at 37°C to remove the loosely attached microglia. Following this, an additional 16–17 hr of shaking was done to obtain the OPCs. To further purify the cells collected, we adopted a differential adhesion method (25 min) on untreated Petri dishes. Purified OPCs were then seeded at a density of 45,000 and cultured for 14 days in myelin medium containing DMEM (high glucose, L-glutamine, pyruvate):neurobasal (50:50), NS21, 1% Pen/Strep, GlutaMAX supplement, ITS, 10 ng/mL biotin, 5 μg/mL N-acetylcysteine (NAC) and SATO (100 μg/mL BSA, 60 ng/mL progesterone, 16 μg/mL putrescine, 400 ng/mL T3 and T4).

In Vitro Myelin Sheath Quantification

A myelin sheath is defined as a continuous, smooth tube of MBP staining surrounding a fiber. To measure the length of myelin sheaths on fibers, MBP signals were traced along individual fibers using 40× magnification confocal images (Zeiss LSM800). To compute the number of myelin sheaths per cell, MBP$^+$ cells in the miR-219/miR-338 and Neg miR groups from three independent experiments were included in the analysis. All measurements and counting were done using Fiji.

Scaffold Fabrication

The PCLEEP copolymer (weight-average molecular weight [Mw] = 59,102; number-average molecular weight [Mn] = 25,542) was synthesized according to a procedure described previously,[14] and a

Fiber Diameter Quantification

Scaffolds were sputter-coated with platinum (JFC-1600; JEOL) at 10 mA for 120 s and observed under the scanning electron microscope (JSM-6390 LA; JEOL) at an accelerating voltage of 10 kV. The average fiber diameter was determined using ImageJ (NIH, USA) by measuring 100 fibers per sample from high-magnification (5,000×) scanning electron microscope images.

Scaffold Degradation

Scaffolds (2.35 ± 0.15 mg) (n = 8) were completely immersed in 1 mL of PBS and incubated at 37°C. At each time point, the weight of the hydrated scaffold was measured. The percentage of collagen degradation was then calculated using the following equation.

$$Percent\ of\ collagen\ degradation\ (\%) = \frac{Initial\ mass\ of\ scaffold\ (mg) - Mass\ of\ scaffold\ measured\ at\ each\ time\ point\ (mg)}{Initial\ mass\ of\ scaffold\ (mg)} \times 100\%$$

two-pole air gap electrospinning technique was used to obtain the aligned PCLEEP fibers.[19] In brief, the electrospinning solution was obtained by dissolving PCLEEP in TFE (35% w/v) and loaded into a 3-mL syringe that was capped with a 21G blunt-tipped needle. The solution was charged at +12 kV and extruded at a flow rate of 1.1 mL/hr. The PCLEEP fibers were deposited within a 5-cm air gap area between two stationary collector poles that were charged at −4 kV. Each set of fibers was obtained after 75 s of electrospinning. Four sets of fibers were then sterilized under UV light for 45 min and set in place within a sterilized cylinder mold (5 mm in length and 4.5 mm in inner diameter). 200 μL of rat tail collagen type 1 was then prepared to a concentration of 3 mg/mL following manufacturer's protocol and added into the mold. Hydrogel formation took place at room temperature for 30 min. The scaffolds were then frozen at −20°C for 3 hr before being lyophilized overnight. Finally, the scaffolds were cut into 1-mm-long pieces and sterilized under UV light for 45 min before *in vivo* implantation.

Drug Loading

NT-3 was loaded into all the scaffolds and delivered together with the miRs. For calculations regarding NT-3 incorporation into the scaffolds, distilled (DI) water within the collagen mixture was replaced with 1 μL of NT-3 (stock concentration is 2 μg/μL, 2 μg per scaffold for implantation), which was, in turn, reconstituted in 0.1% BSA and heparin (400 μg/μL) (1:1 v/v). For calculations regarding miR incorporation, miR (2 μg per scaffold containing equal parts of miR-219, miR-338-3p, and miR-338-5p) and TKO (1:1 v/v) were complexed for 15 min at room temperature. After complexation, the solution was then added into the collagen mixture. For the control scaffold, Neg miR was used to complex with TKO instead.

Drug Release Kinetics

The release kinetics of miR and NT-3 from the scaffolds was evaluated under static conditions. Neg miR- and NT-3-incorporated scaffolds were incubated in 1.2 mL of 1× TE buffer and PBS, respectively, at 37°C. Three samples (2.08 ± 0.15 mg) were used. At each time point, 600 μL of buffer was collected from each sample and replaced with an equal volume of fresh buffer. The amount of NT-3 released over time was determined using an NT-3 ELISA assay. For miR quantification, to each of the supernatants collected, 100 μL of 100 mg/mL heparin was added and thoroughly mixed at 130 rpm for an hour to decomplex Neg miR from TKO. The concentration of miR that was released into the supernatant was then quantified using Quant-iT RiboGreen assay following manufacturer's protocol.

In order to retrieve the remaining Neg miR and NT-3 from the scaffolds at the end of the release kinetics study, the scaffolds were submerged in collagenase for 1 hr at 37°C. Upon complete dissolution of the collagen, the supernatant was tested for NT-3 using ELISA, whereas miR samples were decomplexed with heparin as described above and analyzed using Quant-iT RiboGreen RNA reagent kit. The loading efficiency of the drugs was then computed respectively using the following equation.

$$Loading\ Efficiency = \frac{Total\ drug\ released + Total\ drug\ extracted}{Total\ theoretical\ drug\ loaded} \times 100\%$$

Animals

All animals were obtained from In Vivos Pte (Singapore). The animal care and experimental procedures were carried out in accordance to

Table 1. Experimental Groups

	No. of Animals (n)		
Group	Week 1	Week 2	Week 4
Neg miR + NT-3	3	8	7
miR-219/miR-338 + NT-3	4	5	7
NT-3 only	–	4	–

the Institutional Animal Care and Use Committee (IACUC, NTU) guidelines. Animals were housed under temperature-controlled conditions, with a normal 12/12 hr light/dark cycle with *ad libitum* access to water and food.

SCI Surgical Procedures

Thirty-eight adult female (7–9 weeks, 180–230 g) Sprague-Dawley rats were used as outlined in Table 1. Buprenorphine (0.05 mg/kg) was administered to each animal subcutaneously 30 min before surgery. Anaesthesia was then induced using a 4%–5% mixture of isoflurane in air followed by intraperitoneal injection of ketamine (75 mg/kg) and xylazine (10 mg/kg). Once deeply anaesthetized, the dorsal region of the rats (cervical to pectoral) was shaved and cleaned with 70% ethanol and betadine. A midline incision was made at the disinfected area, and the overlying muscles were bluntly dissected to expose the C5-C6 vertebrae. A laminectomy procedure was further performed to reveal the underlying spinal cord. Following that, the dura was sliced open and a one-third right lateral incision was made on the spinal cord. The scaffold (1 mm in length) was then implanted into the lesion site once the bleeding had subsided. After the implantation, a piece of fat tissue was used to cover the injury, the muscles were sutured using Prolene 4/0 single stitches, and the skin was closed using wound clips. Post-operative treatments included subcutaneous injection of buprenorphine (0.05 mg/kg) and addition of meloxicam (5 mg/mL) into the drinking water.

Immunohistochemical Analysis

At designated time points post-implantation, animals were deeply anesthetized with an intraperitoneal injection of sodium pentobarbital (100 mg/kg) before being transcardially perfused with 0.9% saline solution followed by 4% paraformaldehyde (PFA). The implanted scaffolds and some of the surrounding spinal cord tissues were then harvested and further transferred into 4% PFA for 2 hr, followed by 15% sucrose solution for 24 hr, and finally 30% sucrose solution. Thereafter, the tissues were embedded in Tissue-Tek O.C.T. Compound and cut into 20-μm-thick horizontal sections using a cryostat (Leica CM1950). Immunofluorescent staining was performed to evaluate the effects of the treatment on various cell types of interest. Sections were permeabilized with 0.3% Triton X-100, blocked with 10% goat serum for 1 hr, and incubated with primary antibodies overnight at room temperature. Primary antibodies used included mouse anti-CC-1 (1:200 dilution), rabbit anti-Olig2 (1:200 dilution), rabbit anti-PDGFRα (1:3,000 dilution; gift from Prof. Stallcup), rat anti-MBP (1:200 dilution), chicken

anti-NF200 (1:1,000 dilution), mouse anti-CNPase (1:1,000 dilution), and rabbit anti-GFAP (1:1,000 dilution). After primary antibody incubation, the samples were washed thrice with PBS before secondary antibody incubation for 1 hr at room temperature, using the following: goat anti-mouse Alexa Fluor 555 (1:1,000 dilution), goat anti-rat Alexa Fluor 555 (1:1,000 dilution), goat anti-rat Alexa Fluor 633 (1:500 dilution), goat anti-rabbit Alexa Fluor 488 (1:7,000 dilution), and goat anti-chicken Alexa Fluor 488 (1:700 dilution). Finally, nuclei were labeled with DAPI (1:1,000 dilution), and all slides were coverslipped with Mowiol.

Quantification for the number of DAPI, Olig2, PDGFRα, and CC-1-positive cells in the tissue samples was conducted using a fluorescently labeled stitched collage consisting of several 10× magnified images (Leica DMi8). The region of interest was defined to be 100 μm around the lesion site (Figure 3A), and cells were manually counted using ImageJ cell counter (NIH, USA). To quantify myelination index in the implant interface and within the scaffold, we used 40× magnified z stacks obtained from Zeiss LSM800 along with a colocalization software from ImageJ (NIH, USA). A total of three spinal cord sections were used for quantification per animal. The myelination index is defined by the following equation.

$$Myelination\ Index(\%) = \frac{Number\ of\ overlapping\ NF200\ and\ MBP\ pixels}{Number\ of\ NF200\ pixels} \times 100\%$$

Statistical Analysis

Quantification data were tested for normality and homogeneity of variances using Shapiro-Wilk and Levene's tests, respectively. Data with homogeneous variances were analyzed using one-way ANOVA followed by Tukey's *post hoc* test. Kruskal-Wallis test followed by Mann-Whitney *post hoc* test were used instead for non-parametric data. Error bars represent SEM, unless otherwise stated. The p values obtained from Olig2^{+}, PDGFRα[+], and CC1^{+} cell density comparison within the various groups are displayed in Table S1.

SUPPLEMENTAL INFORMATION

Supplemental Information includes Supplemental Materials and Methods, six figures, and one table and can be found with this article online at https://doi.org/10.1016/j.ymthe.2018.11.016.

CONFLICTS OF INTEREST

The authors declare no competing interests.

REFERENCES

1. Almad, A., Sahinkaya, F.R., and McTigue, D.M. (2011). Oligodendrocyte fate after spinal cord injury. Neurotherapeutics 8, 262–273.

2. Miron, V.E., Kuhlmann, T., and Antel, J.P. (2011). Cells of the oligodendroglial lineage, myelination, and remyelination. Biochim. Biophys. Acta 1812, 184–193.

3. Lee, Y., Morrison, B.M., Li, Y., Lengacher, S., Farah, M.H., Hoffman, P.N., Liu, Y., Tsingalia, A., Jin, L., Zhang, P.W., et al. (2012). Oligodendroglia metabolically support axons and contribute to neurodegeneration. Nature 487, 443–448.

4. Franklin, R.J.M., and Ffrench-Constant, C. (2017). Regenerating CNS myelin—from mechanisms to experimental medicines. Nat. Rev. Neurosci. 18, 753–769.

5. Sasaki, M., Li, B., Lankford, K.L., Radtke, C., and Kocsis, J.D. (2007). Remyelination of the injured spinal cord. Prog. Brain Res. 161, 419–433.

6. Emery, B. (2010). Regulation of oligodendrocyte differentiation and myelination. Science 330, 779–782.

7. Cao, Q., He, Q., Wang, Y., Cheng, X., Howard, R.M., Zhang, Y., DeVries, W.H., Shields, C.B., Magnuson, D.S., Xu, X.M., et al. (2010). Transplantation of ciliary neurotrophic factor-expressing adult oligodendrocyte precursor cells promotes remyelination and functional recovery after spinal cord injury. J. Neurosci. 30, 2989–3001.

8. Crawford, A.H., Tripathi, R.B., Foerster, S., McKenzie, I., Kougioumtzidou, E., Grist, M., Richardson, W.D., and Franklin, R.J. (2016). Pre-existing mature oligodendrocytes do not contribute to remyelination following toxin-induced spinal cord demyelination. Am. J. Pathol. 186, 511–516.

9. Keirstead, H.S., and Blakemore, W.F. (1997). Identification of post-mitotic oligodendrocytes incapable of remyelination within the demyelinated adult spinal cord. J. Neuropathol. Exp. Neurol. 56, 1191–1201.

10. Li, N., and Leung, G.K. (2015). Oligodendrocyte precursor cells in spinal cord injury: a review and update. BioMed Res. Int. 2015, 235195.

11. Emery, B. (2010). Transcriptional and post-transcriptional control of CNS myelination. Curr. Opin. Neurobiol. 20, 601–607.

12. He, L., and Hannon, G.J. (2004). MicroRNAs: small RNAs with a big role in gene regulation. Nat. Rev. Genet. 5, 522–531.

13. Diao, H.J., Low, W.C., Lu, Q.R., and Chew, S.Y. (2015). Topographical effects on fiber-mediated microRNA delivery to control oligodendroglial precursor cells development. Biomaterials 70, 105–114.

14. Diao, H.J., Low, W.C., Milbreta, U., Lu, Q.R., and Chew, S.Y. (2015). Nanofiber-mediated microRNA delivery to enhance differentiation and maturation of oligodendroglial precursor cells. J. Control. Release 208, 85–92.

15. Dugas, J.C., Cuellar, T.L., Scholze, A., Ason, B., Ibrahim, A., Emery, B., Zamanian, J.L., Foo, L.C., McManus, M.T., and Barres, B.A. (2010). Dicer1 and miR-219 Are required for normal oligodendrocyte differentiation and myelination. Neuron 65, 597–611.

16. Zhao, X., He, X., Han, X., Yu, Y., Ye, F., Chen, Y., Hoang, T., Xu, X., Mi, Q.S., Xin, M., et al. (2010). MicroRNA-mediated control of oligodendrocyte differentiation. Neuron 65, 612–626.

17. Wang, H., Moyano, A.L., Ma, Z., Deng, Y., Lin, Y., Zhao, C., Zhang, L., Jiang, M., He, X., Ma, Z., et al. (2017). miR-219 cooperates with miR-338 in myelination and promotes myelin repair in the CNS. Dev. Cell 40, 566–582.e5.

18. Plemel, J.R., Keough, M.B., Duncan, G.J., Sparling, J.S., Yong, V.W., Stys, P.K., and Tetzlaff, W. (2014). Remyelination after spinal cord injury: is it a target for repair? Prog. Neurobiol. 117, 54–72.

19. Nguyen, L.H., Gao, M., Lin, J., Wu, W., Wang, J., and Chew, S.Y. (2017). Three-dimensional aligned nanofibers-hydrogel scaffold for controlled non-viral drug/gene delivery to direct axon regeneration in spinal cord injury treatment. Sci. Rep. 7, 42212.

20. Milbreta, U., Nguyen, L.H., Diao, H., Lin, J., Wu, W., Sun, C.-Y., Wang, J., and Chew, S.Y. (2016). Three-dimensional nanofiber hybrid scaffold directs and enhances axonal regeneration after spinal cord injury. ACS Biomater. Sci. Eng. 2, 1319–1329.

21. Ong, W., Lin, J., Bechler, M.E., Wang, K., Wang, M., Ffrench-Constant, C., and Chew, S.Y. (2018). Microfiber drug/gene delivery platform for study of myelination. Acta Biomater. 75, 152–160.

22. Bechler, M.E., Byrne, L., and Ffrench-Constant, C. (2015). CNS myelin sheath lengths are an intrinsic property of oligodendrocytes. Curr. Biol. 25, 2411–2416.

23. Hollis, E.R., 2nd, and Tuszynski, M.H. (2011). Neurotrophins: potential therapeutic tools for the treatment of spinal cord injury. Neurotherapeutics 8, 694–703.

24. Yokoo, H., Nobusawa, S., Takebayashi, H., Ikenaka, K., Isoda, K., Kamiya, M., Sasaki, A., Hirato, J., and Nakazato, Y. (2004). Anti-human Olig2 antibody as a useful immunohistochemical marker of normal oligodendrocytes and gliomas. Am. J. Pathol. 164, 1717–1725.

25. Matsubayashi, Y., Iwai, L., Toda, T., Lu, Q.R., and Kawasaki, H. (2009). Immunostaining for oligodendrocyte-specific galactosphingolipids in fixed brain sections using the cholesterol-selective detergent digitonin. J. Neurosci. Methods 178, 87–98.

26. Barres, B.A., and Raff, M.C. (1994). Control of oligodendrocyte number in the developing rat optic nerve. Neuron 12, 935–942.

27. McTigue, D.M., Horner, P.J., Stokes, B.T., and Gage, F.H. (1998). Neurotrophin-3 and brain-derived neurotrophic factor induce oligodendrocyte proliferation and myelination of regenerating axons in the contused adult rat spinal cord. J. Neurosci. 18, 5354–5365.

28. Thomas, A.M., Seidlits, S.K., Goodman, A.G., Kukushliev, T.V., Hassani, D.M., Cummings, B.J., Anderson, A.J., and Shea, L.D. (2014). Sonic hedgehog and neurotrophin-3 increase oligodendrocyte numbers and myelination after spinal cord injury. Integr. Biol. 6, 694–705.

29. Alizadeh, A., and Karimi-Abdolrezaee, S. (2016). Microenvironmental regulation of oligodendrocyte replacement and remyelination in spinal cord injury. J. Physiol. 594, 3539–3552.

30. Fitch, M.T., and Silver, J. (2008). CNS injury, glial scars, and inflammation: inhibitory extracellular matrices and regeneration failure. Exp. Neurol. 209, 294–301.

31. Lau, P., Verrier, J.D., Nielsen, J.A., Johnson, K.R., Notterpek, L., and Hudson, L.D. (2008). Identification of dynamically regulated microRNA and mRNA networks in developing oligodendrocytes. J. Neurosci. 28, 11720–11730.

32. Kondo, T., and Raff, M. (2000). Basic helix-loop-helix proteins and the timing of oligodendrocyte differentiation. Development 127, 2989–2998.

33. Liu, A., Li, J., Marin-Husstege, M., Kageyama, R., Fan, Y., Gelinas, C., and Casaccia-Bonnefil, P. (2006). A molecular insight of Hes5-dependent inhibition of myelin gene expression: old partners and new players. EMBO J. 25, 4833–4842.

34. Wang, X., Ding, B., and Li, B. (2013). Biomimetic electrospun nanofibrous structures for tissue engineering. Mater Today (Kidlington) 16, 229–241.

35. Hesp, Z.C., Goldstein, E.Z., Miranda, C.J., Kaspar, B.K., and McTigue, D.M. (2015). Chronic oligodendrogenesis and remyelination after spinal cord injury in mice and rats. J. Neurosci. 35, 1274–1290.

36. Assinck, P., Duncan, G.J., Plemel, J.R., Lee, M.J., Stratton, J.A., Manesh, S.B., Liu, J., Ramer, L.M., Kang, S.H., Bergles, D.E., et al. (2017). Myelinogenic plasticity of oligodendrocyte precursor cells following spinal cord contusion injury. J. Neurosci. 37, 8635–8654.

37. Lee, S., Chong, S.Y.C., Tuck, S.J., Corey, J.M., and Chan, J.R. (2013). A rapid and reproducible assay for modeling myelination by oligodendrocytes using engineered nanofibers. Nat. Protoc. *8*, 771–782.

38. Michailov, G.V., Sereda, M.W., Brinkmann, B.G., Fischer, T.M., Haug, B., Birchmeier, C., Role, L., Lai, C., Schwab, M.H., and Nave, K.A. (2004). Axonal neuregulin-1 regulates myelin sheath thickness. Science *304*, 700–703.

39. Taveggia, C., Thaker, P., Petrylak, A., Caporaso, G.L., Toews, A., Falls, D.L., Einheber, S., and Salzer, J.L. (2008). Type III neuregulin-1 promotes oligodendrocyte myelination. Glia *56*, 284–293.

40. Theodore, N., Hlubek, R., Danielson, J., Neff, K., Vaickus, L., Ulich, T.R., and Ropper, A.E. (2016). First human implantation of a bioresorbable polymer scaffold for acute traumatic spinal cord injury: a Clinical pilot study for safety and feasibility. Neurosurgery *79*, E305–E312.

41. Zhao, Y., Tang, F., Xiao, Z., Han, G., Wang, N., Yin, N., Chen, B., Jiang, X., Yun, C., Han, W., et al. (2017). Clinical study of NeuroRegen scaffold combined with human mesenchymal stem cells for the repair of chronic complete spinal cord injury. Cell Transplant. *26*, 891–900.